On-line monitoring of the electric arc-spraying process based on acoustic signatures

R Kovacevic, MS, PhD, MemASME, MAWS, MSME, **R Mohan**, BS, MS, MemASME, MSME, MAWS,
M Murugesan, MS, MSME and **A F Seybert**, MS, PhD, MemASME, MASA
Department of Mechanical Engineering and Center for Robotics and Manufacturing Systems, University of Kentucky, Lexington, Kentucky, USA

Electric arc spraying (or metal arc spraying) is a process that deposits metal particles on suitable substrates using two consumable wire electrodes. The high-temperature arc formed between these electrodes in an atomizing jet of air produces small molten particles which are used to coat the substrate. The contribution of the process parameters and their interactions on the coating thickness is analysed using Taguchi's design of experiments. The time and frequency domain sound signals generated during the process are utilized to characterize the spraying phenomenon. Stochastic modelling of acoustic signals forms the basis for a closed-loop control mechanism of the arc-spraying process proposed for the first time. Experimental proof of the Gaussian nature of the deposition profile is provided and a mathematical approach has been suggested to obtain a uniform deposit thickness in a single pass.

Key words: electric arc spraying process, atomizing jet, Taguchi's design of experiments, stochastic modelling of acoustic signals

NOTATION

a_t	random noise
A, B, C, D	process parameters for Taguchi's design of experiments.
e	exponential function (value = 2.718 281 828)
E	r.m.s. error of Gaussian fitting
$f(x)$	Gaussian distribution function
F	F-testing ratio
G	Green's function peak
G_j	Green's function
h_1	deposit thickness to be achieved per pass
h_2	predicted deposit thickness using sound signals
Δh	height to be compensated = $h_1 - h_2$
H	required thickness to be sprayed
Δi	compensating current for height Δh
I	current
m	number of passes
N	total number of points for Gaussian distribution
P	pressure
$P\%$	percentage contribution
RE	relative error
SS	sum of squares
v	velocity of arc spray gun
V_A	variance of parameter A
x	point along the X axis
X	distance between two deposits = $2n\sigma$
y	maximum height of Gaussian profile
$\hat{y}_i$	Gaussian fitting value of deposit height for each x
$\tilde{y}_i$	experimental value of deposit height for each x
Y_i	observations of data from $i = 1$ to N
γ	degrees of freedom
$\Theta_1, \ldots, \Theta_3$	moving average coefficients
μ	mean of Gaussian distribution
π	3.141 592 654
σ	standard deviation of Gaussian distribution
σ_a^2	variance of white noise
$\Phi_1, \ldots, \Phi_4$	autoregressive coefficients

1 INTRODUCTION

Coatings of high-performance materials like metals, alloys, ceramics or carbides on suitable substrates can be obtained using the thermal spraying process. There are different thermal spraying processes such as plasma, electric arc, high-energy plasma, vacuum, flame and high-velocity oxy-fuel (HVOF) spray.

The thermal spraying process (initially known as powder spraying) was developed around 1910 to produce metal powders when molten metal was poured on to rapidly rotating wheels. Growth of this process was relatively slow until the late 1950s. Thermal spraying has found widespread applications in recent years. It is being used to spray high-performance materials on the stationary and rotating parts of aircraft engines, recovery boilers, ceramic varistors, cylinder linings, etc. Thermal spraying is also utilized in the chemical processing industry for coating reactors, pipes and vats with anticorrosive materials. While plasma spraying constitutes nearly 50 per cent of the total spray applications, other technologies like electric arc spraying and HVOF are being increasingly used due to their dependability and low cost factor.

Electric arc spraying or metal arc spraying uses two consumable wire electrodes to apply metal to suitable substrates. These wire electrodes are fed into a spray gun where they meet and form an arc in an atomizing jet of air. Due to the high temperature produced by the arc the wire electrodes melt to form small molten particles. The jet of air disintegrates these particles which adhere to the substrate to form a uniform coating. The

substrate temperatures are low and the whole process is energy efficient, since the energy input per pound of metal is only about one-eighth of other spray methods (1).

Several investigations have been conducted to study the electric arc-spraying process. The momentum transfer between the atomizing air and the molten spray particles was numerically simulated by Busse (2). The thermal and kinetic behaviour of the particles was studied by Busse and Sobbe (3). Hohle *et al.* (4) used a high-speed camera to prove that the larger particles are broken into smaller particles after the arc formation. Wagner and Kminek (5) found that the arc current is an important factor in the arc and particle formation.

Much work has been done to integrate electric arc spraying, as a manufacturing unit for prototype parts, with computer aided design. Weiss *et al.* (6) have developed a system called the mask and deposit (MD) system where the arc spraying forms a part of a CAD/CAM (computer aided design/manufacture) integration unit. Production of uniform thickness forms an important part in this integration system. Fasching *et al.* (7) have suggested that the deposition profile is Gaussian for a stationary spray gun and have hypothesized that with a track gap of one standard deviation a uniform deposit thickness can be obtained through several passes.

Indirect sensing of different manufacturing processes has been accomplished very effectively using acoustic signals. The metal-cutting process was monitored using pattern recognition analysis of sound radiation (8). Bhat *et al.* (9) studied the effect of ultrasonic sound signals on the physical characteristics and imperfections of flame-sprayed coatings. Nozzle wear in plasma cutting torches was monitored by Braeuel *et al.* (10) using the amplitude and spectral structure of the resonant tone. Acoustic signal data were used by Kovacevic *et al.* (11) to determine nozzle wear in the abrasive waterjet cutting process. Study of plasma initiation and propagation during laser beam welding was performed by monitoring the sound intensity (12). A real-time weld acoustic monitor was developed for gas metal arc welding by Matteson *et al.* (13).

Similar to the above attempts, the acoustic signals generated in the electric arc-spraying process can be used to provide more information about the arcing phenomenon. The variation of sound signals with change in process parameters can be monitored to reduce the inconsistencies in the deposit thickness caused by the instability of the process. In this paper a parametric evaluation is conducted initially to find the percentage contribution of the parameters on the deposit height using Taguchi's design for experiments (14). Acoustic signals have been used to determine the effect of arc current and atomizing air pressure on the deposit thickness. The microhardness graphs are also studied to obtain more insight into the arching phenomenon. Dynamic characterizing of the arc-spraying process is performed through time series analysis of acoustic data using the ARMA modelling technique (15). This characterization provides the background for the on-line monitoring system proposed for the first time for the electric arc-spraying process. The Gaussian nature of the deposition profile is verified experimentally. A mathematical approach has been suggested for obtaining a layer of uniform thickness in a single pass.
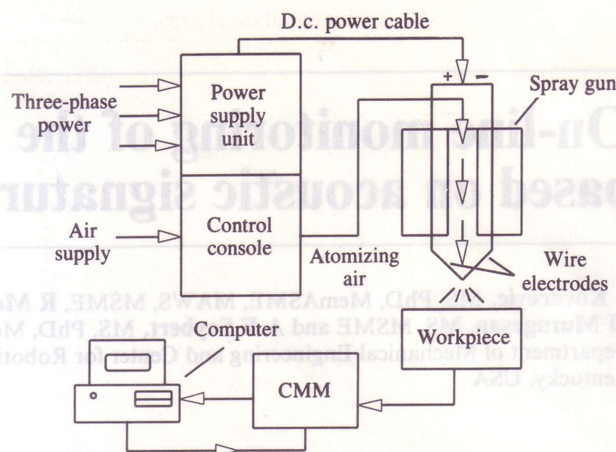
Fig. 1 Experimental set-up for phase 1

2 EXPERIMENTAL SET-UP AND PROCEDURE

All experiments were conducted for a stationary spray gun using a TAFA 8830 arc spray gun with a 200 A power supply unit and a slot type of positioner (Fig. 1). The substrate used for arc spraying was a $150 \times 150 \times 25.4$ mm mild steel plate. The wire material was 204 M Tafalloy™ which is primarily a zinc-based alloy. The substrate surface was prepared by grit blasting and sprayed with TAFA adhesive liquid for better adhesive strength. The specifications of the wire used are shown in Table 1.

The experiments were conducted in two phases. The first phase consists of experiments performed according to Taguchi's orthogonal array (OA), as shown in Table 2. The experimental set-up (Fig. 1) includes the electric arc spray system, a CNC (computer numerically controlled) coordinate measuring machine (CMM), a computer and the workpiece. The deposit height (thickness) was measured using the CMM. An analysis of variance (ANOVA) was performed to quantify the percentage contribution of the process parameters on deposit thickness.

The second phase was performed to determine the influence of process parameters on the deposit height

Table 1 Process parameters

Specifications of wire	
Manufacturer	Hobart TAFA
Material	204 M Tafalloy™
Wire diameter	2.00 mm
Melting point	422°C
Parameters for phase 1	
Arc current	75–125 A
Atomizing air pressure	413–482 kPa
Stand-off distance	203–254 mm
Time of spray	20 s
Parameters for phase 2	
Arc current	75–125 A
Atomizing air pressure	413–482 kPa
Stand-off distance	228 mm
Time of spray	30 s

Table 2 L8 orthogonal array

Trial number	1	2	3	4	5	6	7	Deposit height mm
1	1	1	1	1	1	1	1	6.33
2	1	1	1	2	2	2	2	8.29
3	1	2	2	1	1	2	2	7.87
4	1	2	2	2	2	1	1	9.48
5	2	1	2	1	2	1	2	4.26
6	2	1	2	2	1	2	1	4.61
7	2	2	1	1	2	2	1	5.30
8	2	2	1	2	1	1	2	7.13

Column 1: stand-off distance (level 1, 203 mm; level 2, 254 mm).
Column 2: arc current (level 1, 75 A; level 2, 125 A).
Column 3: interaction between stand-off distance and arc current.
Column 4: air pressure (level 1, 413 kPa; level 2, 482 kPa).
Column 5: interaction between stand-off distance and air pressure.
Column 6: interaction between arc current and air pressure.
Column 7: error function.

and the generated acoustic signals. The experimental set-up for this phase, shown in Fig. 2, includes the arc-spraying system, a 6.35 mm condenser microphone, amplifier, computer with signal processor and the workpiece. The coordinate points of the deposition profile were measured using the CMM. The maximum height was determined through a computer program. A frequency range of 0–20 kHz (audible range) was used for the sound signals. Sampling time for a single sweep of frequency range was 200 ms and 10 data sets were averaged to obtain the FFT (fast Fourier transform).

3 RESULTS AND DISCUSSION

The results of Taguchi's design of experiments (phase 1) were used to find the percentage contribution of the chosen process parameters and their interactions on the deposit height. An attempt has been made to relate the variation of sound generated by the process to the variation in deposit thickness at different parameter settings (phase 2). The frequency domain sound signals were analysed to provide more insight into the stability and intensity of the arc. The results in phase 2 were also used to characterize the shape of the deposition for a stationary spray gun and an analytical method has been suggested to obtain a layer of uniform thickness in a single pass.

3.1 Percentage contribution of process parameters on deposit thickness

The design of experiments is an important aspect of parametric study of any manufacturing process, which may be composed of a multitude of parameters and

their interactions affecting the process. The variation of the output should be measured and the effect of parameters on this variation should be determined. Taguchi (14) has come up with some fractional factorial experiments (FFE) which enable the effect of process parameters and their interactions on the output to be quantified.

An L8 OA (Table 2) has been used, taking into consideration the different procedures recommended by Taguchi (14), in forming the experimental design. Three main factors, namely arc current, atomizing air pressure and stand-off distance and their interactions at two different levels, were considered for the OA. An ANOVA is conducted for the results obtained from the experiments performed according to the OA. The results of the ANOVA are given in Table 3. The stand-off distance is found to be the most influential parameter on the deposit thickness, accounting for nearly 60 per cent of the total contribution. The arc current and the atomizing air pressure account for 20 and 17 per cent respectively. The interactions have only a minor influence. The error function contribution is just 1.75 per cent, indicating that no important factor was excluded from the experiments. These results have a confidence level of 90 per cent.

Due to the differences in initial droplet trajectory and turbulent mixing with ambient air, the spray pattern diverges with an increase in stand-off distance. Simple geometry dictates that a given volume of material spread over a larger area will have a lower peak thickness. All droplets start with a zero initial velocity as they melt from the wire. Initially, they are accelerated by the atomizing air until they reach the ambient gas velocity and then decelerate. The particles are in their decelerating mode at the stand-off distance chosen for study (2). Thus stand-off distance forms the most dominant parameter in determining the deposit thickness.
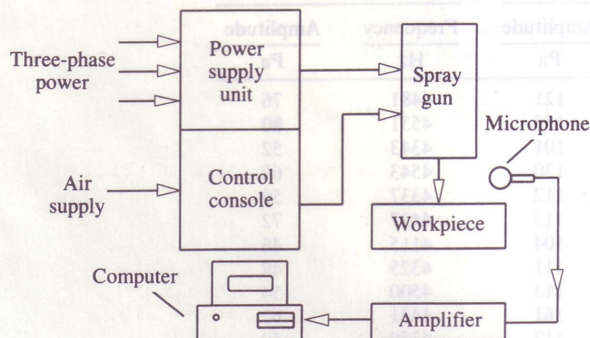
The current is found to be more influential than the atomizing air pressure. This is because the wire feed rate, which is directly proportional to the arc current (16), determines the quantity of the molten metal. However, there is an optimum current setting above which the deposit thickness decreases. This aspect is discussed in detail later.

The interaction between the stand-off distance and the atomizing air pressure is relatively high. This influence is more prominent than the influence of other interactions because of the combined effect of the air pressure and stand-off distance on the velocity of the particles.

Table 3 Results of Taguchi's parameter design

Source	SS	γ	V	F*	P%
A	0.022 08	1	0.022 08	1924.23	58.74
B	0.007 67	1	0.007 67	1000.64	20.4
C	0.006 43	1	0.006 43	955.05	17.11
D	0.000 65	1	0.000 65	805.82	1.73
BC	0.000 25	1	0.000 25	796.39	0.665
AB	0.000 13	1	0.000 13	568.21	0.345
AC	0.000 38	1	0.000 38	798.98	1.011
Total	0.037 59	7	—	—	100

A = stand-off distance; B = arc current; C = atomizing air pressure; D = error function; SS = sum of squares; Source = parameter and interaction; γ = degrees of freedom; F* = F-testing ratio (90% confidence); P% = percentage contribution; V = variance.
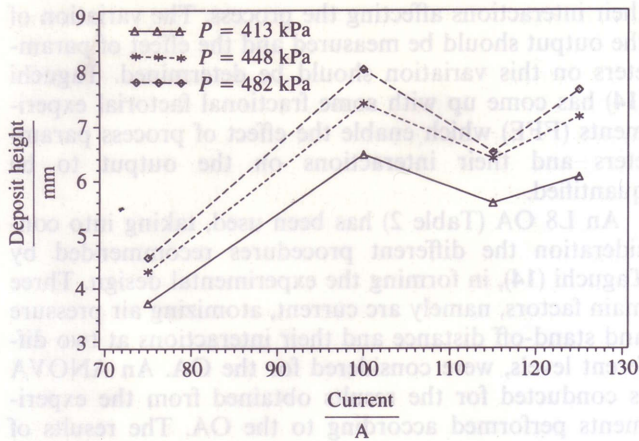

Fig. 2 Experimental set-up for phase 2

Fig. 3 Plot of deposit height for varying current at constant air pressure

Fig. 4 Plot of deposit height for varying air pressure at constant current

3.2 Influence of process parameters on deposit thickness

Preliminary studies indicated that the sound generated might be useful in providing more insight into the influence of the process parameters on the arc formation and hence the deposit thickness. Thus experiments were conducted by changing the arc current and atomizing air pressure with a constant stand-off distance. Results of Taguchi's design for experiments (described above) indicated that deposit thickness is very sensitive to a change in stand-off distance. This high sensitivity is undesirable for feedback control mechanisms. Also, the acoustic signal as a parameter for feedback control is not sensitive to a change in stand-off distance as it is generated by the arcing process. Hence, stand-off distance was not considered as a variable parameter for this investigation (phase 2). Once the initial setting of stand-off distance, arc current and atomizing air pressure is made, the feedback control can be performed by controlling the arc current or atomizing air pressure.

The frequency domain sound signals are found to provide good insight into the behaviour of the arc at various parameter settings. The change in the amplitude is reflected indirectly on the deposit thickness. The variation of the deposit thickness with change in arc current and atomizing air pressure are shown in Figs 3 and 4 respectively. Typical frequency domain graphs are shown in Fig. 5. The amplitudes of primary and secondary frequencies of the sound signals are given in Table 4.
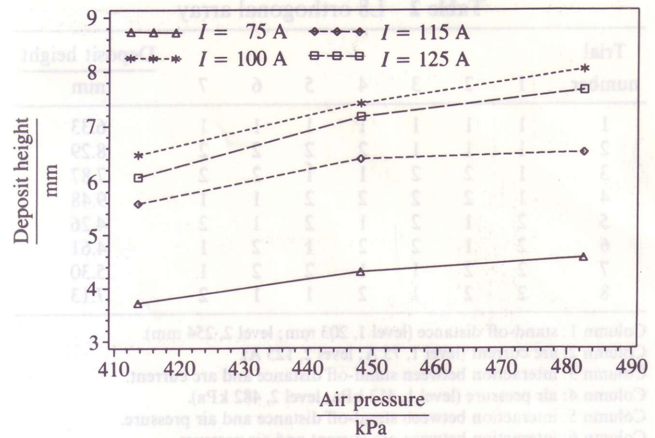
3.2.1 Arc current

For all cases of air pressure, when the current is varied the deposit thickness follows a cubic relationship, as shown in Fig. 4. The maximum deposit thickness is reached at 100 A, after which there is a fluctuation. These changes can be attributed to the stability and intensity of the arc at the point of arc formation by studying the frequency domain data.

It is expected that as arc current increases, the intensity of the arc will also increase, leading to a higher deposit thickness. An increase in arc current causes a higher metal feed rate (16), which leads to more molten metal formation, resulting in higher deposit thickness. This positive effect of the formed molten metal exists till 100 A. However, it is found from the graphs that at 115 A there is a distinct drop in the deposit thickness. This decrease in thickness can be attributed to intermittent and unstable arc caused by the presence of more molten metal at the arc-formation zone. As the current increases beyond 125 A, the deposit height also increases because the mass of the material being melted is more, resulting in an increase in the momentum of the particles. Even though a higher deposit thickness is obtained, the process is less stable at 125 A than at 100 A. Thus, although an increase in feed rate is more desirable as it contributes to higher deposit thickness, beyond an optimum current of 100 A the higher metal feed rate has a negative influence on the arc stability

Table 4 Primary and secondary frequency of sound signals

| | | | Primary | | Secondary | |
| | Current | Pressure | Frequency | Amplitude | Frequency | Amplitude |
Number	A	kPa	Hz	Pa	Hz	Pa
1	75	413	1312	121	4481	76
2	100	413	1318	155	4531	80
3	115	413	1312	101	4343	52
4	125	413	1281	130	4543	62
5	75	448	1312	112	4337	59
6	100	448	2025	113	4437	72
7	115	448	2025	104	4115	46
8	125	448	1700	111	4325	49
9	75	482	1312	113	4500	54
10	100	482	1325	161	4431	62
11	115	482	1318	117	4350	59
12	125	482	1343	192	4515	61

(a) Constant air pressure, varying current
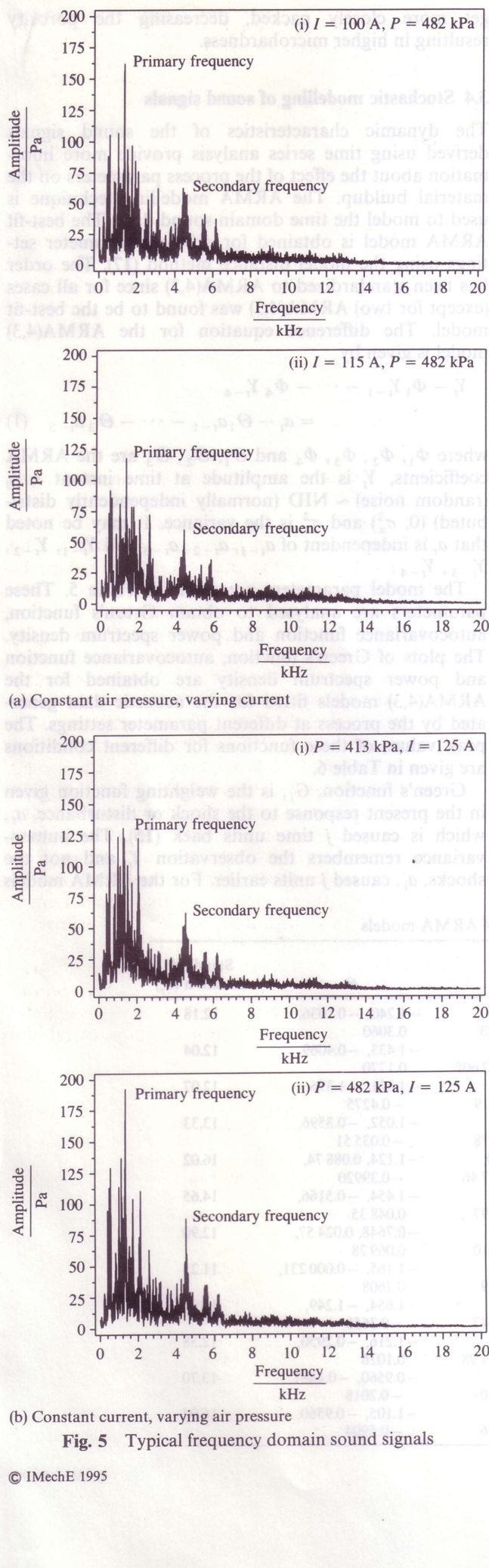

(b) Constant current, varying air pressure

Fig. 5 Typical frequency domain sound signals

which affects the efficiency of the metal spraying process.

The stability factor can also be explained by analysing the change in amplitude and frequency of the sound signals. When current increases from 75 to 100 A the amplitude of the acoustic signal increases for both primary and secondary frequencies. The value of the frequency also increases. This increase in amplitude and shifts in frequencies indicate a stable arc condition which is responsible for the increase in deposition height. The amplitude drops down at 115 A and again increases at 125 A. No change is found in the primary frequency but the secondary frequency shows a distinct drop of about 200 Hz when the current exceeds 100 A. There is an increase in the frequency again at 125 A for all cases. The fluctuations of the deposit height above 100 A is well reflected by the amplitude and the frequency shifts. Thus, it can be concluded that the stability of the arc and hence the buildup of material on the substrate is affected by the arc current.

3.2.2 Atomizing air pressure

Figure 4 shows that with an increase in atomizing air pressure the deposit height also increases linearly for all currents. As air pressure increases the momentum transfer between the atomizing air and the molten particles increases, which results in better adherence of the particles at a constant stand-off distance. At higher pressures, the atomizing air passing through the slot-type positioner directs the particles towards the centre, which increases the deposit height.

The frequency domain sound signals obtained with and without arcing are helpful in explaining the trend shown by deposit height as pressure increases. Hence experiments were performed with and without arcing to determine the effect of air pressure on the sound signals. It was found that with an increase in air pressure there is an increase in the amplitude of the primary and secondary frequencies for both cases, reflecting the increase of deposit height. This confirms the existence of higher velocity and higher momentum transfer, which are given as reasons for the increase of material buildup. As there are no noticeable frequency shifts in all these cases it can be concluded that the atomizing air pressure has no influence on the stability of the arc.

3.3 Influence of process parameters on microhardness

The instability of the arc after 100 A is further confirmed by studying the microhardness graphs shown in Fig. 6. As current increases from 75 to 100 A, the microhardness also increases. There is a prominent drop in the microhardness at 115 A for all air pressure settings. Due to the arc instability at 115 A, the particles are not evenly distributed. Also, the particles may not be of uniform size, leading to inconsistent deposition of material. This affects the adherence of the particles resulting in lower microhardness.

It can be seen from Fig. 7 that as pressure increases for constant currents, there is a linear increase in the microhardness. This is similar to the trend shown by the deposit height for an increase of air pressure at constant currents. It is known that as air pressure increases the
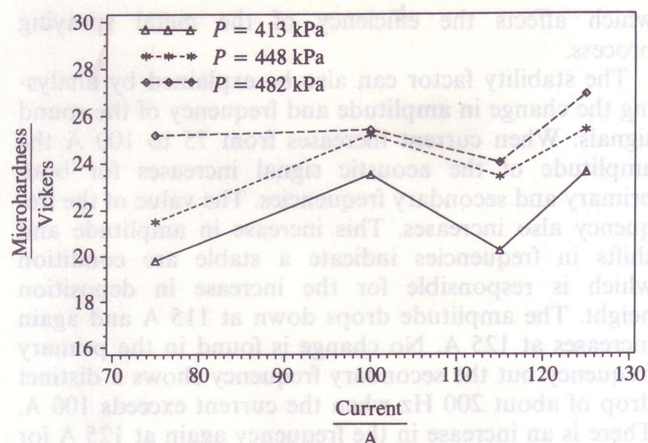
Fig. 6 Plot of microhardness for varying current at constant air pressure

velocity of the particles increases. It has been shown by Hohle *et al.* (**4**) through experimental studies that an increase in pressure leads to more disintegration of the particles, reducing the droplet size. Hence the particles
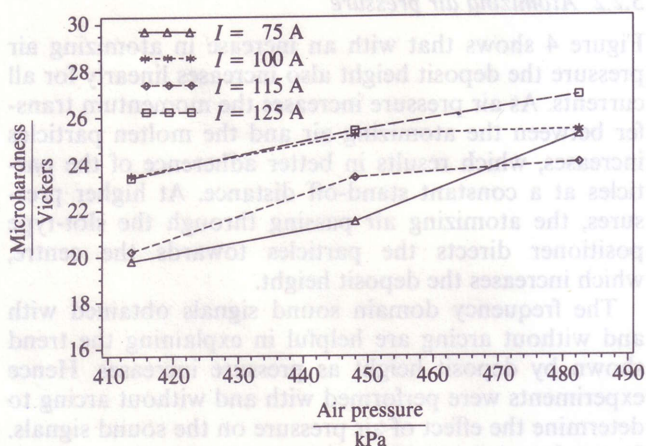

Fig. 7 Plot of microhardness for varying air pressure at constant current

get more closely packed, decreasing the porosity resulting in higher microhardness.

3.4 Stochastic modelling of sound signals

The dynamic characteristics of the sound signals derived using time series analysis provide more information about the effect of the process parameters on the material buildup. The ARMA modelling technique is used to model the time domain sound data. The best-fit ARMA model is obtained for different parameter settings using the model distance method (**17**). The order has been standardized to ARMA(4,3) since for all cases (except for two) ARMA(4,3) was found to be the best-fit model. The difference equation for the ARMA(4,3) model is given by

$$Y_t - \Phi_1 Y_{t-1} - \cdots - \Phi_4 Y_{t-4}$$
$$= a_t - \Theta_1 a_{t-1} - \cdots - \Theta_3 a_{t-3} \quad (1)$$

where Φ_1, Φ_2, Φ_3, Φ_4 and Θ_1, Θ_2, Θ_3 are the ARMA coefficients, Y_t is the amplitude at time instant t, a_t (random noise) $\sim$ NID (normally independently distributed) $(0, \sigma_a^2)$ and σ_a^2 is the variance. It may be noted that a_t is independent of a_{t-1}, a_{t-2}, a_{t-3} and Y_{t-1}, Y_{t-2}, Y_{t-3}, Y_{t-4}.

The model parameters are given in Table 5. These parameters are analysed to obtain Green's function, autocovariance function and power spectrum density. The plots of Green's function, autocovariance function and power spectrum density are obtained for the ARMA(4,3) models fitted for the acoustic data generated by the process at different parameter settings. The peak values of these functions for different conditions are given in Table 6.

Green's function, G_j, is the weighting function given in the present response to the shock or disturbance, a_t, which is caused j time units back (**15**). The autocovariance remembers the observation Y_t and not the shocks, a_t, caused j units earlier. For the ARMA models

Table 5　Parameters of ARMA models

Number	Current A	Pressure kPa	Φ	Θ	Standard deviation (σ_y)
1	75	413	1.323, −0.4922, 0.054 37, 0.0123	−1.240, −0.1036, 0.3060	12.18
2	75	448	1.175, −0.4667, 0.1326, −0.002 602	−1.433, −0.4069, 0.1770	12.04
3	75	482	1.168, −0.7687, 0.6627, −0.2919	−1.821, −1.376, −0.4275	12.07
4	100	413	1.371, −0.8811, 0.4506, −0.1278	−1.052, −0.3596, −0.035 51	13.33
5	100	448	1.655, −0.902 10, 0.2158, −0.047 46	−1.124, 0.088 74, −0.392 20	16.02
6	100	482	1.470, −0.9773, 0.5845, −0.2497	−1.454, −0.5166, 0.048 35	14.65
7	115	413	1.715, −1.407, 0.8678, −0.3110	−0.7648, 0.024 57, 0.069 28	12.90
8	115	448	1.562, −1.098, 0.544, −0.1519	−1.165, −0.000 231, 0.2608	11.25
9	115	482	1.206, −0.9225, 0.8194, −0.3347	−1.654, −1.249, −0.3658	11.69
10	125	413	1.252, −0.5368, 0.1822, −0.031 98	−1.216, −0.2950, 0.1026	12.38
11	125	448	1.476, −1.172, 0.7823, −0.2708	−0.9560, −0.4481, −0.2018	13.70
12	125	482	1.392, −1.271, 1.174, −0.4776	−1.105, −0.9560, −0.5904	16.04

Table 6 System dynamics

Number	Current A	Pressure kPa	Deposit height mm	Green's function peak	Auto-covariance peak	Power spectrum peak
1	75	413	3.72	2.80	24.0	2044
2	75	448	4.30	2.85	25.8	2030
3	75	482	4.57	2.88	27.8	1972
4	100	413	6.47	3.10	29.0	2998
5	100	448	7.41	3.60	51.0	4196
6	100	482	8.04	4.80	46.0	2020
7	115	413	5.58	2.90	25.8	2030
8	115	448	6.40	3.10	27.0	2387
9	115	482	6.52	3.20	30.0	1315
10	125	413	6.06	2.98	25.0	3642
11	125	448	7.17	3.20	45.5	4533
12	125	482	7.66	3.80	50.0	2762

both Green's function and the autocovariance function represent the same phenomenon, namely the dependence of an observation on the preceding observations in time.

A similar trend in Green's function and autocovariance (except for one case) corresponding to the deposit height can be seen. The peak of Green's function and the autocovariance is at 100 A for all pressure settings. Moreover, the peaks of these functions drop at 115 A and again increase at 125 A. Since the trends shown by these dynamic characteristics and the deposit heights are similar it can be concluded that the data are dependent on the previous observations at a magnitude that is proportional to the deposit height and hence the deposition rate. With an increase of air pressure for constant currents, it can be found that the trend followed by the deposit height, Green's function and the autocovariance function, with the exception of one case, is again similar. Since Green's function and the autocovariance are complementary, Green's function is taken to be the primary parameter for analysis even though the autocovariance can also be considered. Thus Green's function can be used to give an indication about the deposit height for on-line monitoring of the arc-spraying process.

The power spectrum density is the Fourier cosine transform of the autocovariance function. It does not indicate a clear trend in relation to the deposit height like Green's function or the autocovariance function.

3.5 Closed-loop control mechanism for arc-spraying process

Based on the dynamic characteristics of the acoustic signals, an on-line monitoring and control mechanism has been proposed (18) for the first time for the arc-spraying process. This mechanism is capable of ensuring that the desired deposit thickness can be achieved under optimized conditions.

The number of passes needed to achieve a desired thickness (H) is initially determined. The range of the deposit height h_1 for one layer of uniform coating is known from the experiments previously performed. This height h_1 is required to find the number of passes needed to achieve a particular thickness H. For the experiments conducted over a pressure range of 413–482 kPa and a current range of 75–125 A, the range of

h_1 was found to be 3.72–8.04 mm. Thus, the number of passes m can be obtained from the following equation:

$$H = mh_1 \qquad (2)$$

where m is an integer value.

The first step in the control loop is to have an initial setting of the control parameters. This initial setting is determined based on the relationship between the deposition height and the process parameters, namely arc current and air pressure. The suitable parameter is chosen and the corresponding pressure (or current) is determined from the graphs depicting the relationship between the deposit height and these parameters (Fig. 3 or Fig. 4). The spraying process is initiated and the sound signals generated by the process are measured for the corresponding parameter setting. Time series analysis is performed using ARMA modelling and the parameters of the best-fit model are obtained. Green's function peak varies similarly to the deposit height with an increase in arc current at a constant atomizing air pressure. Hence the current is varied at one chosen air pressure and the relationship between Green's function and the deposition height is obtained. This relationship for a pressure of, say, 482 kPa is given by

$$h_2 = 3.3G^3 - 38.7G^2 + 151.2G - 188 \qquad (3)$$

Based on this relationship, h_2 is predicted and is compared with h_1. The difference, $\Delta h = h_1 - h_2$, is to be compensated by changing the current at constant air pressure. A relationship is required between the current and Δh, in which the current is the dependent variable. For an air pressure of 482 kPa, this relationship is given by

$$\Delta i = -13\Delta h^3 + 239\Delta h^2 - 1425\Delta h + 2827 \qquad (4)$$

The compensation is made by changing the current for constant air pressure conditions and the control loop is completed.

3.6 Determination of deposition profile

It can be noted that the above-mentioned closed-loop control mechanism can ensure the required thickness of sprayed layer. However, there is an increasing need to obtain a uniform layer of deposition. Towards this, the profile of the spray deposit for a fixed spray gun is to be

determined. Fasching *et al.* (7) have suggested that this profile is Gaussian in shape. However, no experimental proof was provided to verify this hypothesis. This aspect is investigated here using the samples collected from the experiments conducted in phase 2. The coordinates of the samples were measured using the CMM and the profile of the deposition was determined. This profile was compared with an ideal Gaussian curve and the relative error was obtained. The ideal Gaussian profile can be represented mathematically by

$$f(x) = \frac{\exp[-\frac{1}{2}\{(x - \mu)/\sigma\}^2]}{\sigma\sqrt{(2\pi)}} \qquad (5)$$

where σ is the standard deviation of the distribution ($\sigma > 0$) and μ is the mean.

The r.m.s. error of the Gaussian fitting can be defined as

$$E = \sqrt{\left\{\frac{\sum_{i=1}^{N} (\hat{y}_i - \tilde{y}_i)^2}{N}\right\}} \qquad (6)$$

where $\hat{y}_i$ is the Gaussian fitting value obtained using equation (5) for each x, $\tilde{y}_i$ is the experimental data for the corresponding x and N is the total number of points for the distribution. The relative error is given by

$$RE = \frac{E}{\sigma} \times 100\% \qquad (7)$$

A typical graph showing the Gaussian curve and the experimental data is shown in Fig. 8. The relative error, shown in Table 7, varies between 0.01 and 1.3 per cent for different parameter settings. From these experiments, it can be concluded that the distribution of the spray profile obtained for a fixed spray gun is Gaussian in nature, as defined by equation (5) for all·parameter settings.

3.7 Determination of optimal track gap for uniform deposition

Fasching *et al.* (7) have suggested a method to obtain uniform spray deposition by selecting a track gap equal to one standard deviation. For this technique several passes need to be performed in order to achieve a
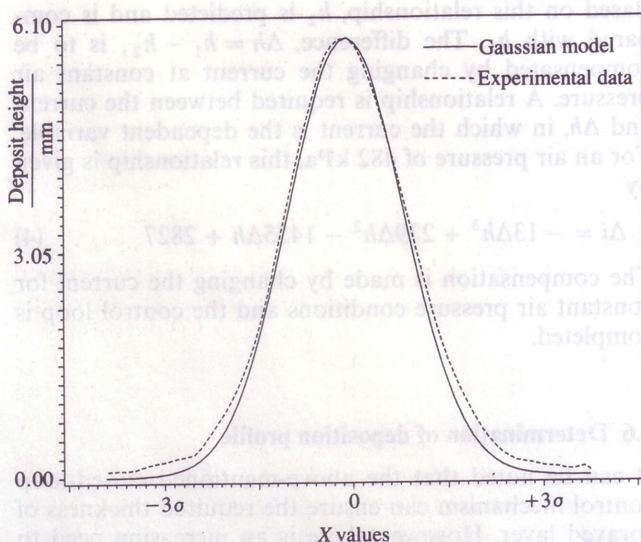

Fig. 8 Comparison between Gaussian fitting and the experimental data

Table 7 R.m.s. error for Gaussian fitting

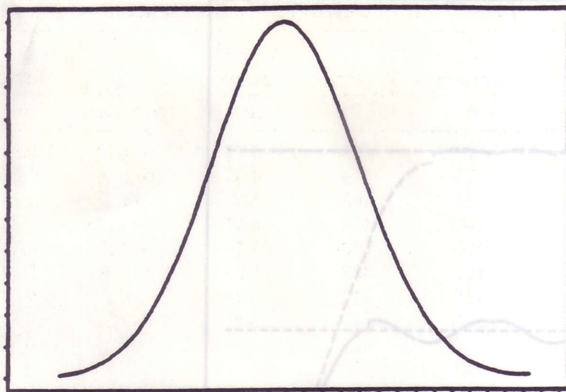| Number	Current A	Pressure kPa	Deposit height mm	Standard deviation	Error %
1	75	413	3.72	0.1072	0.31
2	75	448	4.30	0.0926	0.21
3	75	482	4.57	0.0873	0.39
4	100	413	6.47	0.0616	1.31
5	100	448	7.41	0.0538	0.40
6	100	482	8.04	0.0496	0.64
7	115	413	5.58	0.0715	0.77
8	115	448	6.40	0.0623	0.51
9	115	482	6.52	0.0612	0.56
10	125	413	6.06	0.0658	0.97
11	125	448	7.17	0.0556	0.46
12	125	482	7.66	0.0521	0.70

uniform deposition. A novel approach to this problem is given below which enables a uniform deposition to be obtained in a single pass.

For a continuous spray process, the torch can be assumed to move in the Y direction at a velocity which ensures a deposition of uniform height along that direction. In order to obtain a uniform layer, the spray is stopped and the spray gun is moved to the next position in the X direction. The distance to which the gun moves without spraying is called the track gap. In the absence of an optimum track gap, the amount of material sprayed may not be sufficient to provide a uniform deposition in one pass and hence more passes are required. However, in the method developed here, the track gap is optimized such that it ensures uniform deposition in one pass, eliminating subsequent passes. In this case the spraying parameters will be kept constant during the building-up process of the entire thickness. As a result, the mechanical and physical properties of the buildup will be uniform throughout the thickness.
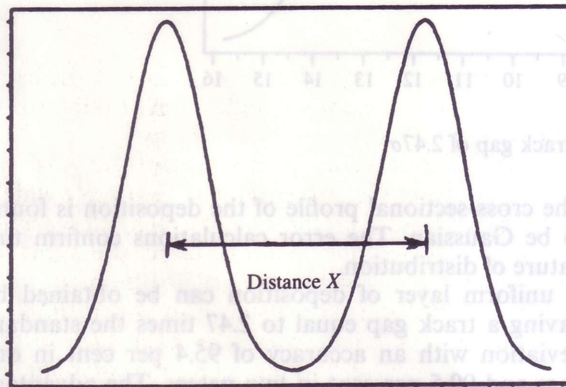
Figure 9a gives a cross-section of one deposition. The three-dimensional shape of the deposition can be visualized as the axisymmetric region generated by rotating this cross-section through 180° about the Z axis. Hence the two-dimensional mathematical approach adopted here is valid for three-dimensional space as well.

It is assumed that two consecutive depositions are at a finite distance, X, as shown in Fig. 9b. From this figure it can be seen that the volume between the two depositions is to be filled to achieve uniform thickness. When the two consecutive depositions are close enough, the material from the second deposition is sprayed on top of the first deposition at the overlapping region. Optimizing this distance X ensures that the sprayed material from the second deposition is capable of filling the volume between depositions completely. Extending this approach to the required number of depositions to cover the entire length to be sprayed would enable a uniform thickness to be obtained in one pass. This is the basic approach adopted here to achieve uniform spray height in one pass.
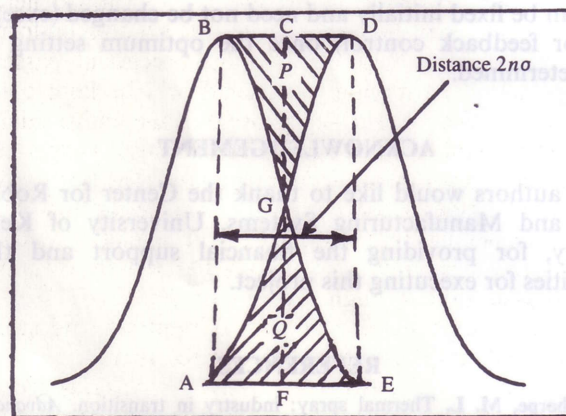
Figure 9c shows two consecutive depositions that are at a distance of $2n\sigma$, where n is a real number. However, in reality, the material from the second deposition is sprayed on top of the overlapping region (indicated by Q) with the first deposition. The valley indicated by the hatched area P is the region devoid of any material,

(a)

Distance X

(b)

Distance $2n\sigma$

(c)

Fig. 9 (a) Cross-section of one deposition
(b) Two consecutive depositions at a finite distance X
(c) Two consecutive depositions at a distance $2n\sigma$

assuming that the two spray depositions are performed independently. In order to achieve uniform spray thickness, the region indicated by P should be equal to the region denoted by Q. The area under the Gaussian curve within the 3σ limit can be assumed to contain 100 per cent of the deposition area. The area of region P is given by

$$P = 2 \,(\text{area of region ABCF} - \text{area of region ABGF})$$
(8)

$$P = 2\left(yn\sigma - \int_{\mu}^{\mu + n\sigma} \frac{\exp[-\frac{1}{2}\{(x - \mu)/\sigma\}^2]}{\sigma\sqrt{(2\pi)}}\,dx \right)$$
(9)

where

$$y = \frac{\exp\{-\frac{1}{2}(\mu/\sigma)^2\}}{\sigma\sqrt{(2\pi)}}$$
(10)

The area of region Q is given by

$$Q = 2 \,(\text{area of region AGDE} - \text{area of region FGDE})$$
(11)

$$Q = 2\left(\int_{\mu}^{\mu + 2n\sigma} \frac{\exp[-\frac{1}{2}\{(x - \mu)/\sigma\}^2]}{\sigma\sqrt{(2\pi)}}\,dx \right.$$
$$\left. - \int_{\mu + n\sigma}^{\mu + 2n\sigma} \frac{\exp[-\frac{1}{2}\{(x - \mu - 2n\sigma)/\sigma\}^2]}{\sigma\sqrt{(2\pi)}}\,dx \right)$$
(12)

For optimum spacing of deposition, the area of region P should be equal to that of region Q. Thus, from equations (9) and (12),

$$yn\sigma = \int_{\mu}^{\mu + 2n\sigma} \frac{\exp[-\frac{1}{2}\{(x - \mu)/\sigma\}^2]}{\sigma\sqrt{(2\pi)}}\,dx$$
(13)

Substituting equation (10) in equation (13),

$$n = \frac{1}{\exp\{-\frac{1}{2}(\mu/\sigma)^2\}} \left(\int_{\mu}^{\mu + 2n\sigma} \frac{\exp[-\frac{1}{2}\{(x - \mu)/\sigma\}^2]}{\sigma}\,dx \right)$$
(14)

It has been determined by the above approach that a uniform thickness is achieved if the nozzle is moved by a distance of 2.47σ between consecutive spray depositions. The uniform deposition is achieved in one pass in this case as opposed to more passes needed in the methods suggested earlier (7). However, it must be kept in mind that in order to achieve a definite spraying thickness, more passes with uniform height are required. The continuous spray process in the Y direction can be approximated as a sum of several discrete depositions performed at a finite deposition rate. Thus, the velocity v of the spray gun in the Y direction, which can provide uniform height of deposition, is given by

$$v = 2.47\sigma \times \text{deposition rate}$$
(15)

The uniformity of the deposition profile obtained using the above method can be measured in terms of the relative error, which is defined as the ratio of the r.m.s. error of the actual deposition profile to the ideal deposit thickness. Contours of the deposition layer obtained in the first pass and second pass for a track gap of 2.47σ are given in Fig. 10a and b respectively. Even though the track gap is the same for both passes, there is an offset of a half track gap between the two passes, as shown in Fig. 10. This provides a more uniform layer after the second pass with a relative error of 0.49 per cent compared to 4.6 per cent after the first pass. Based on the accuracy requirements, one pass or two passes can be adopted at a track gap of 2.47σ to obtain a uniform deposit thickness. Thus, if the number of passes, m in equation (2), is chosen to be an even integer, a uniform layer similar to Fig. 10b with an accuracy of 99.51 per cent can be obtained by having alternate passes at an offset of a half track gap.

An important advantage of this method is that the parameters can be fixed initially and need not be changed until the final layer is obtained. Choosing suitable parameters can ensure an optimum performance of
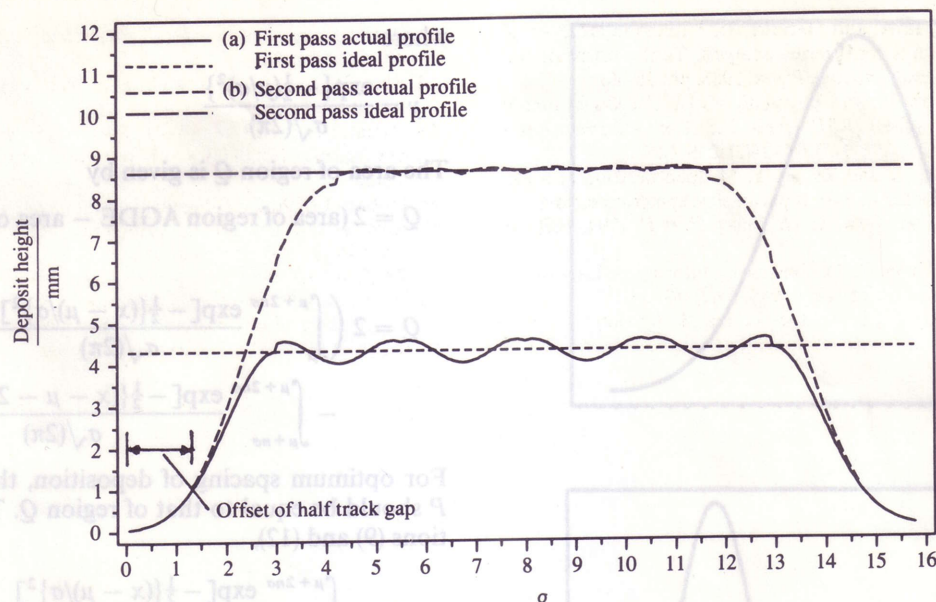
Fig. 10 Deposition profiles for a track gap of 2.47σ

the spraying process. As these parameters are not changed subsequently, except during feedback control, a deposition layer of uniform physical and mechanical properties can be obtained by this approach. Once the spraying process is initialized, as the need to change the parameter setting is eliminated, the process time can be considerably reduced compared to the existing methods.

4 CONCLUSIONS

The conclusions from this investigation can be summarized as follows:

1. By using Taguchi's design of experiments it was found that the stand-off distance accounts for nearly 60 per cent of the total influence on the deposit thickness. The arc current accounts for 20 per cent and the atomizing air pressure contributes to 17 per cent of the total influence. The interactions do not have a significant influence on the deposit height.

2. The sound signals generated by the process were used to find the influence of the arc current and atomizing air pressure. It was found that for all pressure values, the maximum deposit height was reached at 100 A after which, due to the instability of the arc, there were fluctuations in the deposit height. As air pressure increases for constant currents, there is a linear increase in the deposit height, which is due to the increase in momentum of the molten particles. These results are confirmed by the trend of the frequency domain graphs.

3. The microhardness behaves similarly to the deposit height. The adherence of the particles on the substrate is affected by the arc instability above 100 A. The velocity of the particles increases and their size decreases, resulting in higher microhardness with an increase in air pressure for constant arc currents.

4. Dynamic characterization of sound data indicates that the deposit height and Green's function peak follow the same trend for different parameter settings of the current and air pressure. Based on this trend an on-line control mechanism for the arc-spraying process is proposed.

5. The cross-sectional profile of the deposition is found to be Gaussian. The error calculations confirm this nature of distribution.

6. A uniform layer of deposition can be obtained by having a track gap equal to 2.47 times the standard deviation with an accuracy of 95.4 per cent in one pass and 99.5 per cent in two passes. The advantage of using this track gap is that the mechanical and physical properties are optimized and the parameters can be fixed initially and need not be changed (except for feedback control) once the optimum setting is determined.

REFERENCES

1 **Thorpe, M. L.** Thermal spray: industry in transition. *Advanced Mater. Processes*, 1993, **143**(5), 50–61.

2 **Busse, K. H.** A simplified model for atmospheric arc spraying. Second International Conference on *Surface engineering*, Stratford-upon-Avon, June 1987, paper 39.

3 **Busse, K. H.** and **Sobbe, H.** Spray particle behavior during atmospheric arc spraying. Conference on *Thermal spraying*, 1989, pp. 105–117.

4 **Hohle, H. M., Steffens, H. D.** and **Beczkowiak, J.** Optimisation of electric arc and flame spraying conditions by application of high speed cinematography. Tenth International Conference on *Thermal spraying*, Essex, 1983, pp. 148–152.

5 **Wagner, J.** and **Kminek, Z.** The stability of arc-spraying process. Tenth International Conference on *Thermal spraying*, Essex, 1983, pp. 146–147.

6 **Weiss, L. E., Prinz, F. B., Adam, D. A.** and **Siewiorek, D. P.** Thermal spray shape deposition. *J. Thermal Spray Technol.*, September 1992, **1**(13), 231–237.

7 **Fasching, M., Weiss, L. E.** and **Prinz, F. B.** Optimisation of robotic trajectories for thermal shape deposition. Thirteenth International Spray Conference, Orlando, 1992, pp. 221–226.

8 **Traeisi, E.** and **Kannatey-Asibu Jr, H.** Pattern-recognition analysis of sound radiation in metal cutting. *Int. J. Adv. Mfg Technol.*, 1991, **6**, 220–231.

9 **Bhat, H., Zatorski, R. A.** and **Herman, H.** Ultrasonic analysis of flame sprayed coatings–time series analysis. Tenth International Conference on *Thermal spraying*, Essex, 1983, pp. 36–40.

10 **Braeuel, M., Francois, N.** and **Bayoumi, M. M.** Defects in nozzle of plasma cutting torches. *IEEE Trans. Ultrasonics, Ferroelectrics and Frequency Control*, 1987, **UFFC-34**(2), 259–261.

11 **Kovacevic, R., Wang, L.** and **Zhang, Y. M.** Identification of abrasive waterjet nozzle wear based on parametric spectrum estimation of acoustic signal. *Proc. Instn Mech. Engrs, Part B*, 1994, **208**(B3), 173–181.

12 **Lewis, G. K.** and **Dixon, R. D.** Plasma monitoring of laser beam welds. *Weld. Res. Suppl.*, February 1985, **64**(2), 49–54.

13 **Matteson, A. M., Morris, R. A.** and **Raines, D.** An optimal artificial neural network for GMAW arc acoustic classification. Third International Conference on *Trends in welding research*, Gatlinburg, June 1992.

14 **Ross, P. J.** *Taguchi's technique for quality engineering*, 1991 (John Wiley, Chicago).

15 **Pandit, S. M.** and **Wu, S. M.** *Time series and system analysis with applications*, 1983 (John Wiley, New York) (reprinted by Krieger, 1990).

16 **Hobart TAFA.** *TAFA manual for metal arc spraying equipment.*

17 **Kovacevic, R.** and **Zhang, Y. M.** Identification of surface characteristics from large samples. *Proc. Instn Mech. Engrs, Part C*, 1992, **206**(C4), 275–284.

18 **Murugesan, M., Mohan, R., Kovacevic, R.** and **Seybert, A. F.** Characterization of electric arc-spraying process using sound signals. *Trans. ASME, Mfg Sci. Engng*, PED **68**(1).